Enhancement of visible light photocatalytic activities via porous structure of g-C$_3$N$_4$

CrossMark

Mo Zhang, Jing Xu, Ruilong Zong, Yongfa Zhu*

Department of Chemistry, Beijing Key Laboratory for Analytical Methods and Instrumentation, Tsinghua University, Beijing 100084, China

ARTICLE INFO

ABSTRACT

The series porous graphitic carbon nitride (pg-C$_3$N$_4$) materials have been prepared by pyrolysis of dicyandiamide in air using urea as bubble template. The surface area of as-prepared pg-C$_3$N$_4$ was increased from 5.4 to 60 m^2 g^{-1} by increasing the mass ratio of urea/dicyandiamide and calcination temperature. We have found that thus-produced nanostructures can display efficient photocatalytic performance for the photodegradation of methylene blue (MB) and phenol pollutant when energized with visible light. The photocurrent and photocatalytic activities of as-synthesized pg-C$_3$N$_4$ were increased with the higher proportion of urea and calcination temperature under visible light irradiation. Compared with the bulk g-C$_3$N$_4$, the optimum photocatalytic activity of our synthesized pg-C$_3$N$_4$ displays a significant enhancement by a factor of 2.1 and 2.8 for MB and phenol, respectively. The separation and migration efficiency of photogenerated electron–hole pairs were improved by the porous structure, which resulted in the enhancement of photocatalytic performances.

1. Introduction

Recently, photocatalysts are becoming an appealing class of materials owing to their outstanding performance in conversion of solar energy [1–7]. For the purpose of taking full advantages of solar energy, great efforts have been devoted to searching for suitable materials with visible light photocatalytic activities [8,9]. Graphitic carbon nitride (g-C$_3$N$_4$), with narrow band gap and chemical stability, is considered to be a promising visible light active candidate for degradation of organic pollutants, production of H$_2$ and O$_2$ from water and photocatalytic conversion of CO$_2$ [10–13]. However, the photocatalytic activity of bulk g-C$_3$N$_4$ is limited by its low surface area and quantum efficiency. In general, the synthesis of bulk g-C$_3$N$_4$ includes typical mass polymer of nitrogen-rich precursors or monomers. To date, several efforts have been developed to improve the photocatalytic performance of g-C$_3$N$_4$ in terms of introducing heteroatoms [14–17], sensitizing by dyes [18], coupling with semiconductors or polymers [12,13,19–24] and controlling morphology [25–27]. Nevertheless, a simple development of highly efficient g-C$_3$N$_4$ remains a significant challenge.

Porous materials have received much attention in photocatalysis field due to their accessible porous frameworks and large surface areas [28–32]. Compared with bulk g-C$_3$N$_4$, porous g-C$_3$N$_4$ (pg-C$_3$N$_4$) has higher porosity and specific surface area, which

could enhance its mass transfer ability and photocatalytic activity efficiently. This is owing to larger number of active chemical sites exposed on the surface and improved size selectivity in this porous frameworks [14,18,33,34]. Generally, pg-C$_3$N$_4$ could be obtained by template-induced method [35–39]. For example, by evaporation induced self-assembly, pg-C$_3$N$_4$ could be prepared in the soft-templating method. However, there is still some carbon residue from the templating polymers in the product, which might affect its catalytic activity [35]. On the other hand, silica-templating method is also the most important pathway to obtain nanoporous g-C$_3$N$_4$ [36–39]. The desired pg-C$_3$N$_4$ can be successfully replicated by using silica nanoparticles as hard templates. Nevertheless, the process involves removal of the template by aqueous ammonium bifluoride or hydrogen fluoride, which is hazardous, toxic and not environmentally friendly.

Urea can be facilely thermal conversed into pg-C$_3$N$_4$ without tailoring the reaction pressure and atmosphere. The as-prepared pg-C$_3$N$_4$ exhibit stable adsorption and activity for decomposing organic dyes and show a high activity for H$_2$ evolution under visible light irradiation [18,40]. The drawback of this method is the low yield of pg-C$_3$N$_4$, which may limits its practical application. Herein, pg-C$_3$N$_4$ with surface area of 60 m^2 g^{-1} has been produced on large scale by pyrolysis of urea and dicyandiamide in air. As a nontoxic low-cost bubble template, the urea can decompose and generate gas bubble during the reaction and produce porous structure in g-C$_3$N$_4$ film. The surface area and photocatalytic activity of the pg-C$_3$N$_4$ can be controlled by adjusting the mass ratio of urea/dicyandiamide and calcination temperature. With enhanced

* Corresponding author. Tel.: +86 10 6278 3586; fax: +86 10 6278 7601.
  E-mail address: zhuyf@mail.tsinghua.edu.cn (Y. Zhu).

ability of separation and transfer of photogenerated electron–hole pairs in porous structure, the pg-C_3N_4 exhibits much higher activity than bulk g-C_3N_4 for decomposition of methylene blue (MB) and phenol. This investigation might open up new opportunities for an easy synthesis of highly efficient visible-light-active porous structure of g-C_3N_4 with large scale for organic pollutant elimination.

2. Experimental

2.1. Preparation of pg-C_3N_4 photocatalyst

Dicyandiamide and urea were purchased from Sinopharm Chemical Reagent Corp., PR China. All other reagents used in this research were analytically pure and used without further purification. The pg-C_3N_4 was prepared by pyrolysis of urea and dicyandiamide in air atmosphere. The typical preparation of pg-C_3N_4 photocatalysts was as follows: the urea and dicyandiamide was firstly ball milled for 50 min resulting in ultrafine powder (300 rpm) respectively. To investigate the influence of mass ratio of urea on the catalytic activity of pg-C_3N_4, 5 g of milled urea and dicyandiamide (mass fraction of urea was from 10% to 70%) were put in a Muffle Furnace and heated to 530 °C for 4 h to complete the reaction. To investigate the influence of calcination temperature on the catalytic activity of pg-C_3N_4, 3.5 g urea and 1.5 g dicyandiamide were put in a Muffle Furnace and heated to different temperature (520–550 °C). The yellow products were washed with nitric acid (0.1 mol L^{-1}) and deionized water to remove the residue absorbed on the surface of pg-C_3N_4. Then the pure products were dried at 80 °C for 12 h. The yield of the optimum pg-C_3N_4 was about 18%.

2.2. Characterizations

The morphologies and structures of the samples were examined with HITACHI HT7700 transmission electron microscopy (TEM) operated at an accelerating voltage of 100 kV. UV–vis diffuse reflectance spectroscopy (DRS) was carried out on a Hitachi U-3010 UV–vis spectrophotometer using $BaSO_4$ as the reference. The Brunauer–Emmett–Teller (BET) surface area was measured by ASAP 2010 V5.02H. The crystallinity of the as-prepared sample was characterized by X-ray diffraction (XRD) on Bruker D8-advance diffractometer using Cu Kα radiation (λ = 1.5418 Å). The photocurrents were measured on an electrochemical system (CHI 660D, China).

2.3. Photocatalytic experiments

The photocatalytic activities were evaluated by the decomposition of MB under visible light irradiation (λ > 420 nm). Visible irradiation was obtained from a 500 W Xe lamp (Institute for Electric Light Sources, Beijing) with a 420 nm cutoff filter, and the average visible light intensity was 35 mW cm^{-2}. For the photocatalytic experiments, 25 mg of photocatalyst was totally dispersed in an aqueous solution of MB (50 mL, 0.03 mM). Before irradiation, the suspensions were magnetically stirred in the dark for 60 min to get absorption–desorption equilibrium between the photocatalyst and MB. At certain time intervals, 3 mL aliquots were sampled and centrifuged to remove the particles. The concentration of MB was analyzed by recording the absorbance at the characteristic band of 664 nm using a Hitachi U-3010 UV–vis spectrophotometer.

To investigate the transition of photogenerated electrons of pg-C_3N_4, a standard three-electrode cell with a working electrode (as-prepared photocatalyst), a platinum wire as counter electrode, and a standard calomel electrode (SCE) as reference electrode were used in the photoelectric studies. 0.1 M Na_2SO_4 was used as the electrolyte solution. Potentials are given with reference to the SCE. The photoresponses of the photocatalysts as light on and off were

measured at 0.0 V. The working electrodes were prepared as follows: 2 mg of the as-prepared photocatalyst was suspended in 1 mL water to produce a slurry, which was then dip-coated onto a 2 cm × 4 cm indium tin oxide (ITO) glass electrode. Electrodes were exposed to air atmosphere for 12 h to eliminate water and subsequently calcined at 100 °C for 5 h.

2.4. Analyses of the degradation intermediates for MB and phenol

The chromatographic experiments with HPLC-UV/vis system were carried out using an ultraviolet absorbance detector (K 2501) operated at 615 nm (MB) and 270 nm (phenol) coupled to a Venusil XBP-C_{18} (Agela Technologies Inc.) column. Before the analysis, the samples were filtered through millipore discs of 0.45 μm to protect the chromatographic column. The reversed-phase eluent of pH 5.3 buffer (0.1 M ammonium acetate and acetic acid) and acetonitrile (40:60, v/v) was used as mobile phase for MB degradation intermediates analysis. The flow rate was 0.8 mL min^{-1} and the injection volume was 60 μL. The mobile phase used for eluting phenol and its degradation intermediates from the HPLC columns consisted of methanol and water (60:40, v/v) at a flow rate of 1 mL min^{-1}. The HPLC–MS spectrum was obtained using LC–MS (Thermo Fisher LTQ) equipped with a 16 electrospray ionization source (ESI). The scan range was m/z 50–500 in both negative and positive ion 17 mode. HPLC series is equipped with a reversed-phase C_{18} column. The mobile phase used for HPLC experiments was a mixture of methanol and water (60:40, v/v) with a flow rate of 0.8 mL min^{-1}.

3. Results and discussion

3.1. Formation of porous structure

The pg-C_3N_4 materials were prepared by thermal condensation of urea and dicyandiamide in air atmosphere. Gas bubbles, which produced during the process of carbon nitride condensation, played an important role for the production of porous structure. By adjusting the mass ratio of urea/dicyandiamide and calcination temperature, the porous structure of g-C_3N_4 could be successfully controlled. As shown in Fig. 1, the g-C_3N_4 prepared by thermal polymerization of dicyandiamide at 530 °C exhibited bulk morphology (Fig. 1a). With the increase of urea concentration in the precursor and fixed calcination temperature as 530 °C, the pg-C_3N_4 gradually possessed a loose structure and nanopores in the range of 20–50 nm (Fig. 1b–d). The SEM images in Fig. S1 further confirmed the presence of bulk morphology of g-C_3N_4 and loose and porous structures of pg-C_3N_4. Fig. 2a displays the pore size distribution curves of samples determined from the adsorption branch of the isotherms. Increasingly apparent pore distribution could be observed with the addition of urea in the precursor. The majority of nanopores appeared as broad peak at 20–50 nm for pg-C_3N_4, while little pore size distribution could be detected for bulk g-C_3N_4, which was consistent with the result of TEM images. Brunauer–Emmett–Teller (BET) measurements revealed the progressively increasing surface areas of pg-C_3N_4 prepared with increased mass fraction of urea and fixed calcination temperature as 530 °C, which was about 5 times higher than that of bulk g-C_3N_4 prepared by thermal polymerization of dicyandiamide at 530 °C (Fig. 2b). Obviously, the increasing urea may decompose into more bubbles during the thermal polymerization process, leading to the porous structure of pg-C_3N_4.

The porous structure of pg-C_3N_4 can also be adjusted by the calcination temperature. As shown in the TEM (Fig. 3) and SEM (Fig. S6) images of pg-C_3N_4 with increased calcination temperature and fixed mass fraction of urea as 70%, the pg-C_3N_4 displayed more loose and porous structures as the calcination temperature was raised. Moreover, increasingly apparent pore size distribution

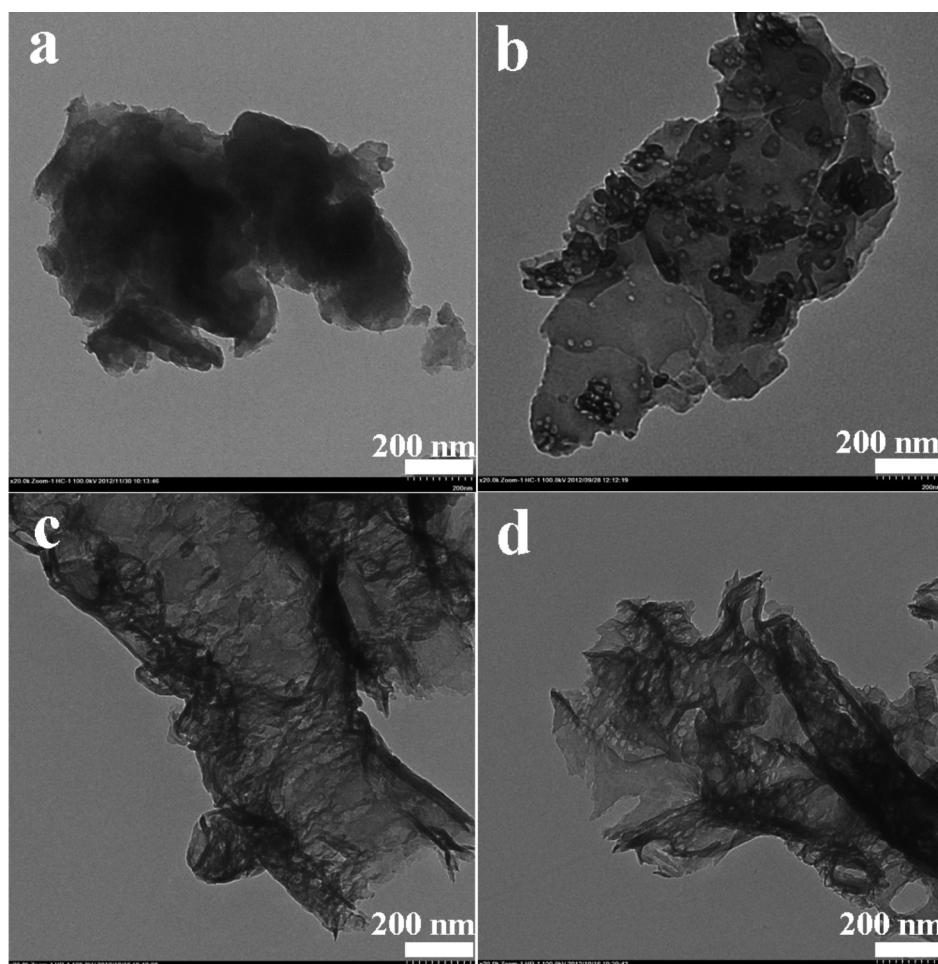**Fig. 1.** TEM images of g-C_3N_4 (a) and pg-C_3N_4 prepared by thermal condensation of precursor with mass fraction of urea as 10%, 50% and 70% (b–d) and fixed calcination temperature as 530 °C.

and surface areas of pg-C_3N_4 could be observed when the reaction temperature went up from 520 °C to 550 °C (Fig. 4). According to the studies on the thermal decomposition of urea, the NH_3 (g), H_2O (g) and CO_2 (g) was the main components of the pyrolysis generated atmosphere [40]. More complete decomposition of urea might be promoted via a higher temperature. Accordingly, the more bubbles were produced during the thermal polymerization process as well. Therefore, it can be estimated that the high mass fraction of urea in the precursor (over the range of 0–70%) and calcination temperature (over the range of 520–550 °C) will be proper to the formation of pore structure and enlargement of surface area.

3.2. Enhancement of photocatalytic activity and photocurrent

The pg-C_3N_4 demonstrated much higher activity than bulk g-C_3N_4 for decomposition of MB and phenol under visible light. Fig. S3 shows the photocatalytic activity of pg-C_3N_4 for decomposition of MB was enhanced gradually with the increasing proportion of urea and fixed calcination temperature as 530 °C. The photocatalytic degradation process was fitted to pseudo-first-order kinetics, and the value of the rate constant k was equal to the corresponding slope of the fitting line. When the mass fraction of urea reached 70%, the as-prepared photocatalyst exhibited the highest photocatalytic
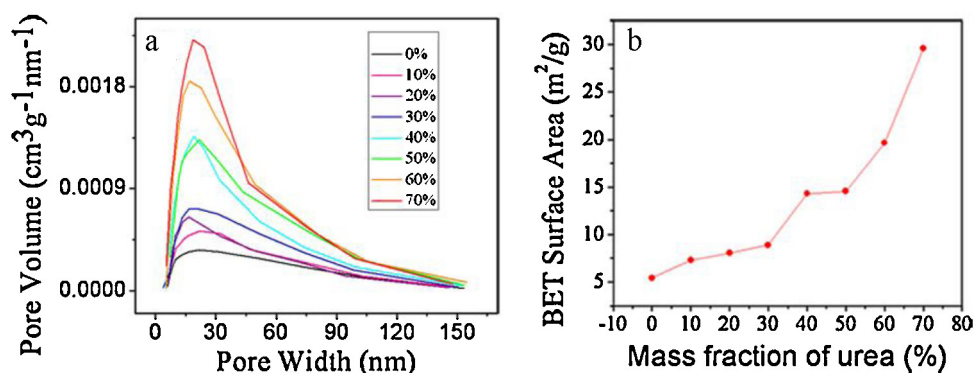

Fig. 2. Pore size distributions (a) and BET specific surface area (b) of pg-C_3N_4 with different mass fraction of urea in precursor and fixed calcination temperature as 530 °C.

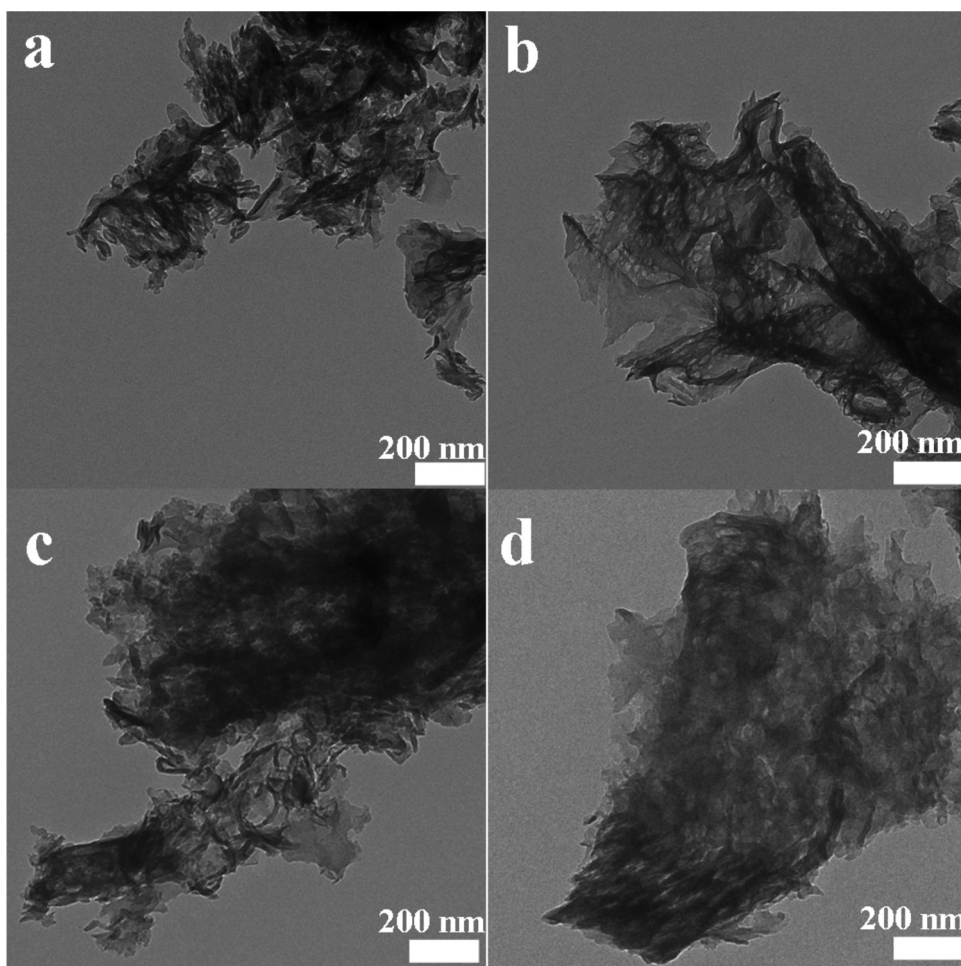**Fig. 3.** TEM images of pg-C$_3$N$_4$ with calcination temperature of 520 °C, 530 °C, 540 °C and 550 °C (a–d) and fixed mass fraction of urea as 70%.

activity. However, when further increasing the proportion of urea, the yield of product could be lower than 10% due to the excessive decomposition of urea during the thermal condensation process. As shown in Fig. S8, the photocatalytic activity was continuously enhanced with rising calcination temperature and fixed mass fraction of urea as 70%. The pg-C$_3$N$_4$ prepared at 550 °C exhibited the best photocatalytic activity, which was 2.1 times as high as that of bulk g-C$_3$N$_4$. Moreover, the pg-C$_3$N$_4$ exhibited higher activity for phenol degradation (Fig. 5c). The rate content of optimum pg-C$_3$N$_4$ for phenol decomposition was 0.039 h^{-1}, which was 2.8 times as high as bulk g-C$_3$N$_4$. This high photocatalytic efficiency was similar

to the decomposition of MB, which revealed that the photocatalytic activity of g-C$_3$N$_4$ could be greatly improved via porous structure.

A responsive photocurrent is used to evaluate the photocatalytic activity of the catalysts. The photocurrent densities as a function of applied potential were investigated by recording current time (I-t) curves and presented in Fig. S4. As shown in Fig. S4, the pg-C$_3$N$_4$ layers coated on ITO glass plates revealed a short circuit photocurrent under visible light illumination (λ > 420 nm). Fast and uniform photocurrent responses were observed in both electrodes and the photoresponsive phenomenon was entirely reversible. Moreover, the value of photocurrent generated from the pg-C$_3$N$_4$ was much
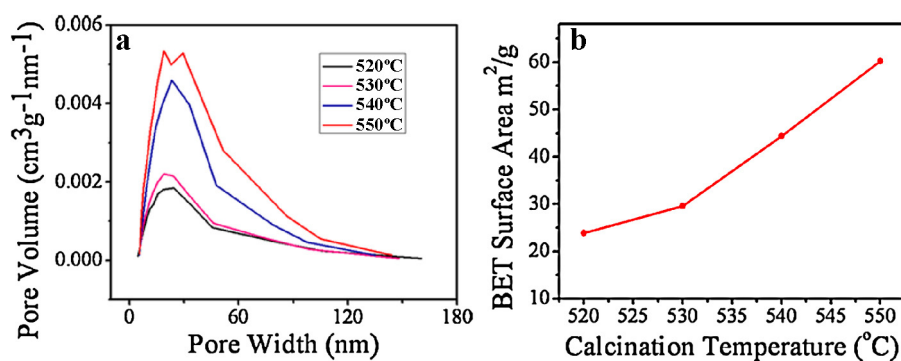

Fig. 4. Pore size distributions (a) and BET specific surface area (b) of pg-C$_3$N$_4$ with calcination temperature of 520 °C, 530 °C, 540 °C and 550 °C and fixed mass fraction of urea as 70%.

Fig. 6. EIS Nyquist plots of pg-C_3N_4 prepared with different precursor (a) and calcination temperature (b) in Na_2SO_4 aqueous solution in the dark and under visible light illumination ($\lambda > 420$ nm, [$Na_2SO_4 = 0.1$ M]).
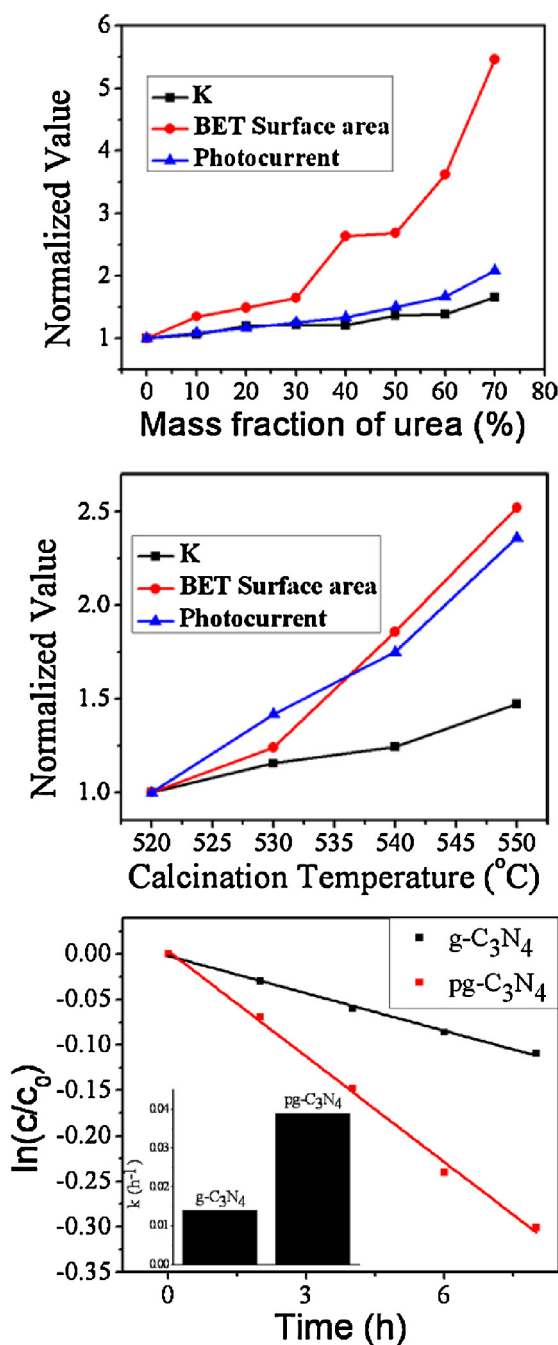

Fig. 5. The normalized value of BET surface area, rate constant of MB degradation (k) and photocurrent of pg-C_3N_4 with the increase proportion of urea in the precursor (a) and calcination temperature (b). The photocatalytic activity of bulk g-C_3N_4 and optimum pg-C_3N_4 for phenol decomposition under visible light irradiation (>420 nm) (c).

higher than bulk g-C_3N_4 and increased gradually with increased mass fraction of urea under calcination temperature at 530 °C, indicating an enhanced photogenerated electrons and holes separation by more loose and porous structures. Fig. S9 shows that the photocurrent of pg-C_3N_4 was gradually enhanced with rising calcination temperature and fixed mass fraction of urea as 70%. The optimum photocurrent was obtained from pg-C_3N_4 prepared with 70% urea and calcination temperature of 550 °C, which was four times as high as that of bulk C_3N_4 (prepared by thermal condensation of pure dicyandiamide at 530 °C) in the same condition. These results indicate that the photocatalytic activity of C_3N_4 can be greatly
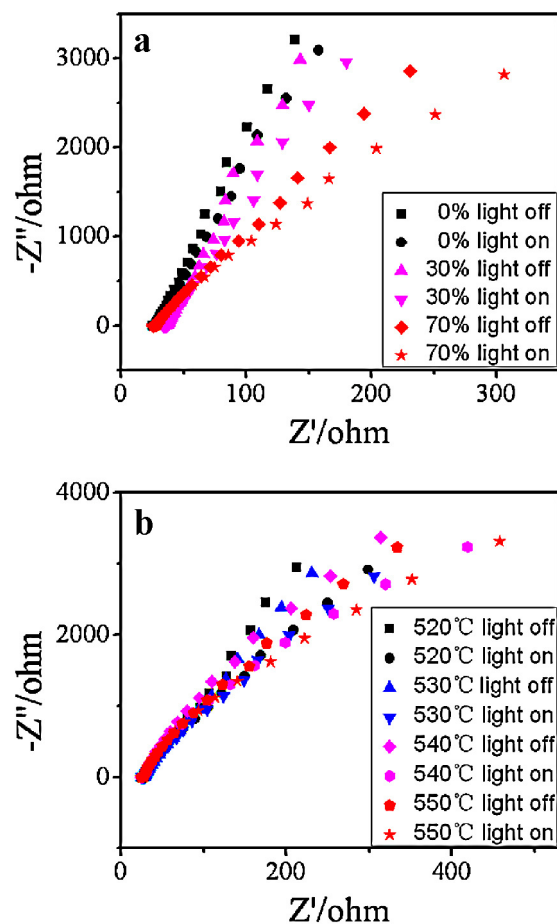
improved by the enhanced photogenerated electrons and holes separation, resulting from the increased porous structure.

Further investigation into the relation between porous structure and photocatalytic activity of pg-C_3N_4 is conducted by comparisons of different measurements. Fig. 5a shows the progressive normalized values of BET surface area, the rate constant of MB degradation (k) and photocurrent of pg-C_3N_4 with incremental proportion of urea in the precursor. (The BET surface area of bulk g-C_3N_4 prepared by thermal condensation of pure dicyandiamide at 530 °C was considered as the reference. The normalized values of BET surface area were obtained by dividing the BET surface area of pg-C_3N_4 by the reference value. The normalized values of k and photocurrent were obtained with the same method.) The increase rate of BET surface area indicated that the transmission distance and recombination rate of photogenerated carriers were reduced and the transportation efficiency was substantially raised along with the expanded pore volume. The improved separation and migration of photogenerated carriers lead to the obviously enhanced catalytic activity of pg-C_3N_4. As shown in Fig. 5b, with fixed urea proportion and rising calcination temperature, the BET surface area was greatly increased by the exhaustive decomposition of urea at higher temperature. The increase of normalized value of BET surface area and photocurrent were larger than that of k. The greater enhancement of photocurrent might be due to the cooperative phenomenon of expanded pore volume and perfect crystallinity (Fig. S7) of pg-C_3N_4 with rising reaction temperature.
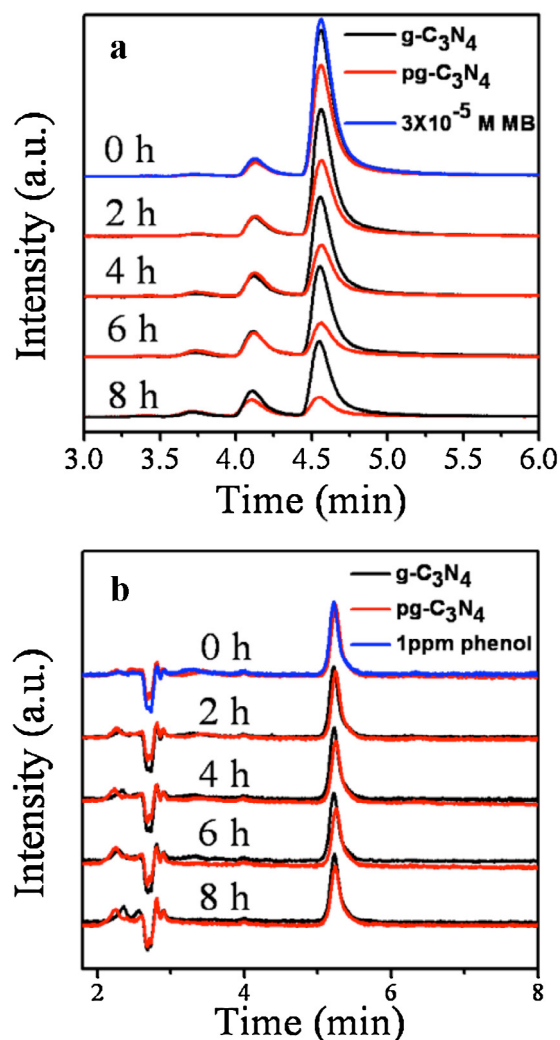
Fig. 7. HPLC chromatograms of MB and after photocatalytic degradation for different irradiation time monitored at 615 nm ([MB] = 3 × 10^{-5} M, catalyst = 25 mg/50 mL) (a) HPLC chromatograms of phenol and after photocatalytic degradation for different irradiation time monitored at 270 nm ([phenol] = 1 ppm, catalyst = 25 mg/50 mL) (b).

3.3. Mechanism of enhanced photocatalytic activity

The separation efficiency of photogenerated electrons and holes is one of the most crucial factors for photocatalytic activity. The charge separation efficiency was investigated by electrochemical impedance spectroscopy (EIS) analysis. The reaction rate occurring on the surface of the working electrode was reflected by the arc radius. Fig. 6 shows the experimental Nyquist impedance plots for bulk g-C_3N_4 and pg-C_3N_4 prepared with different urea proportion and calcination temperature without and with irradiation. The smaller arc radius on the EIS Nyquist plot of pg-C_3N_4 with increased urea content and calcination temperature under visible light irradiation could be observed, indicating that a more effective separation efficiency of photogenerated electron–hole pairs and a faster interfacial charge transfer. The arc radius on the EIS Nyquist plot of pg-C_3N_4 was also smaller than that of bulk C_3N_4 without irradiation, suggesting that the porous structure changed the charge distribution of C_3N_4 and made charge transfer easier. This result implied that higher proportion of urea in the precursor and calcination temperature could obviously favor the separation and transfer of photogenerated carriers in pg-C_3N_4 and then enhanced the photocatalytic activity.

3.4. Degradation mechanism

The chromatographic separation of the MB solution recorded initially and after different irradiation time was monitored at 615 nm. As shown in Fig. 7a, the prominent peak of the MB at 4.57 min was observed to diminish gradually with continuous photocatalytic reaction. The constant of degradation rate of MB by pg-C_3N_4 was 2.3 times as much as bulk g-C_3N_4. The peaks at lower retention times in the spectra indicated that the MB was degraded to several intermediates. The structures of these intermediates were predicted as the cleavage of one or more methyl groups substituent on the amine groups [41–44], thus the process of stepwise degradation of MB was determined. The intensity of new peaks increased to the maximum value and then decreased along with the irradiation time, testifying the degradation ability of C_3N_4 for all the intermediates. The same retention times for the degradation intermediates by bulk g-C_3N_4 and pg-C_3N_4 indicated the identical degraded products. Fig. 7b shows chromatograms of phenol before and after photocatalytic degradation for different irradiation time monitored at 270 nm. The peak at 5.3 min can be identified as phenol, the intensity of which was decreased by degrees during the constant photocatalytic reaction. HPLC-MS results (Figs. S11 and S12) indicate that the degradation reactions of phenol catalyzed by bulk g-C_3N_4 and pg-C_3N_4 followed the same degradation pathway. The main intermediates included dihydroxybenzene, 4,4′-dihydroxybiphenyl and maleic anhydride [45], and they could be further degraded by ring cleavage and finally subjected to completely degradation to CO_2 and H_2O.

4. Conclusions

A facile bubble template method of pyrolysis urea and dicyandiamide for the preparation of porous g-C_3N_4 on large scale was developed. Thus-produced pg-C_3N_4 nanomaterials can display efficient photocatalytic performance for the degradation of MB and phenol under visible light irradiation. Compared with bulk g-C_3N_4, the photocatalytic activity and the intensity of the photocurrent response of pg-C_3N_4 were obviously improved by adjusting the mass fraction of urea in precursor and calcination temperature. This work may shed light on an efficient preparation method for promising porous g-C_3N_4 with large scale and their application in degradation of organic pollutants.

4.1. Supporting information available

Supplementary data (SEM images, XRD patterns, photocatalytic activity, photocurrent, UV–vis diffuse reflectance spectra of g-C_3N_4 and pg-C_3N_4 and HPLC-MS spectrum of the intermediates of phenol degradation by g-C_3N_4 and pg-C_3N_4) associated with this article can be found in the online version.

Appendix A. Supplementary data

Supplementary data associated with this article can be found, in the online version, at http://dx.doi.org/10.1016/j.apcatb.2013.09.002.

References

[1] A. Fujishima, K. Honda, Nature 238 (1972) 37–38.
[2] X. Chen, S. Shen, L. Guo, S.S. Mao, Chem. Rev. 110 (2010) 6503–6570.
[3] S.C. Roy, O.K. Varghese, M. Paulose, C.A. Grimes, ACS Nano 4 (2010) 1259–1278.
[4] M.A. Fox, M.T. Dulay, Chem. Rev. 93 (1993) 341–357.
[5] M.R. Hoffmann, S.T. Martin, W. Choi, D.W. Bahnemann, Chem. Rev. 95 (1995) 69–96.
[6] H. Lee, J. Choi, S. Lee, S.T. Yun, C. Lee, J. Lee, Catal. Appl. B 138–139 (2013) 311–317.
[7] G.S. Shao, X.J. Zhang, Z.Y. Yuan, Catal. Appl. B 82 (2008) 208–218.
[8] Z. Zou, J. Ye, K. Sayama, H. Arakawa, Nature 414 (2001) 625–627.
[9] K. Maeda, K. Teramura, L. Daling, T. Takata, N. Saito, Y. Inoue, K. Domen, Nature 440 (2006) 295–296.
[10] Y. Zheng, J. Liu, J. Liang, M. Jaroniec, S.Z. Qiao, Energ. Environ. Sci. 5 (2012) 6717–6731.
[11] X. Wang, S. Blechert, M. Antonietti, ACS Catal. 2 (2012) 1596–1606.
[12] L. Ge, C. Han, Catal. Appl. B 117–118 (2012) 268–274.
[13] Z. Huang, F. Li, B. Chen, T. Lu, Y. Yuan, G. Yuan, Catal. Appl. B 136–137 (2013) 269–277.
[14] Y. Zhang, T. Mori, J. Ye, M. Antonietti, J. Am. Chem. Soc. 132 (2010) 6294–6295.
[15] X. Chen, J. Zhang, X. Fu, M. Antonietti, X. Wang, J. Am. Chem. Soc. 131 (2009) 11658–11659.
[16] X. Wang, X. Chen, A. Thomas, X. Fu, M. Antonietti, Adv. Mater. 21 (2009) 1609–1612.
[17] G. Liu, P. Niu, C. Sun, S.C. Smith, Z. Chen, G.Q. Lu, H.M. Cheng, J. Am. Chem. Soc. 132 (2010) 11642–11648.
[18] S. Min, G. Lu, J. Phys. Chem. C 116 (2012) 19644–19652.
[19] Y. Wang, R. Shi, J. Lin, Y. Zhu, Energ. Environ. Sci 4 (2011) 2922–2929.
[20] L. Ge, F. Zuo, J. Liu, Q. Ma, C. Wang, D. Sun, L. Bartels, P. Feng, J. Phys. Chem. C 116 (2012) 13708–13714.
[21] L. Ge, C. Han, J. Liu, J. Mater. Chem. 22 (2012) 11843–11850.
[22] C. Pan, J. Xu, Y. Wang, D. Li, Y. Zhu, Adv. Funct. Mater. 22 (2012) 1518–1524.
[23] Y. Wang, X. Bai, C. Pan, J. He, Y. Zhu, J. Mater. Chem. 22 (2012) 11568–11573.
[24] L.W. Zhang, H.B. Fu, Y.F. Zhu, Adv. Funct. Mater. 18 (2008) 2180–2189.
[25] Y.S. Jun, W.H. Hong, M. Antonietti, A. Thomas, Adv. Mater. 21 (2009) 4270–4274.
[26] E.Z. Lee, Y.S. Jun, W.H. Hong, A. Thomas, M.M. Jin, Angew. Chem. Int. Ed. 49 (2010) 9706–9710.
[27] Y. Zhang, A. Thomas, M. Antonietti, X. Wang, J. Am. Chem. Soc. 131 (2008) 50–51.
[28] J.Y. Ying, C.P. Mehnert, M.S. Wong, Angew. Chem. Int. Ed. 38 (1999) 56–77.
[29] G. Soler-Illia, C. Sanchez, B. Lebeau, J. Patarin, Chem. Rev. 102 (2002) 4093–4138.
[30] M. Gratzel, Nature 414 (2001) 338.
[31] Y. Wan, D. Zhao, Chem. Rev. 107 (2007) 2821–2860.
[32] M. Zhou, J. Yu, S. Liu, P. Zhai, B. Huang, Appl. Catal., B 89 (2009) 160–166.
[33] X.H. Li, X. Wang, M. Antonietti, ACS Catal. 2 (2012) 2082–2086.
[34] F. Su, S.C. Mathew, G. Lipner, X. Fu, M. Antonietti, S. Blechert, X. Wang, J. Am. Chem. Soc. 132 (2010) 16299–16301.
[35] W. Shen, L. Ren, H. Zhou, S. Zhang, W. Fan, J. Mater. Chem. 21 (2011) 3890–3894.
[36] A. Vinu, K. Ariga, T. Mori, T. Nakanishi, S. Hishita, D. Golberg, Y. Bando, Adv. Mater. 17 (2005) 1648–1652.
[37] F. Goettmann, A. Fischer, M. Antonietti, A. Thomas, Angew. Chem. Int. Ed. 45 (2006) 4467–4471.
[38] X. Wang, K. Maeda, X. Chen, K. Takanabe, K. Domen, Y. Hou, X. Fu, M. Antonietti, J. Am. Chem. Soc. 131 (2009) 1680–1681.
[39] A. Vinu, Adv. Funct. Mater. 18 (2008) 816–827.
[40] J. Liu, T. Zhang, Z. Wang, G. Dawson, W. Chen, J. Mater. Chem. 21 (2011) 14398–14401.
[41] J. Small, H. Hintelmann, Anal. Bioanal. Chem. 387 (2007) 2881–2886.
[42] M.A. Rauf, M.A. Meetani, A. Khaleel, A. Ahmed, Chem. Eng. J. 157 (2010) 373–378.
[43] C. Yogi, K. Kojima, N. Wada, H. Tokumoto, T. Takai, T. Mizoguchi, H. Tamiaki, Thin Solid Films 516 (2008) 5881–5884.
[44] A. Orendorz, C. Ziegler, H. Gnaser, Appl. Surf. Sci. 255 (2008) 1011–1014.
[45] L. Liu, H. Liu, Y.P. Zhao, Y. Wang, Y. Duan, G. Gao, M. Ge, W. Chen, Environ. Sci. Technol. 42 (2008) 2342–2348.